

# Image Processing Using Multi-Code GAN Prior

Jinjin Gu<sup>1,2</sup>, Yujun Shen<sup>2</sup>, Bolei Zhou<sup>2</sup>

<sup>1</sup>The Chinese University of Hong Kong, Shenzhen <sup>2</sup>The Chinese University of Hong Kong

jinjingu@link.cuhk.edu.cn, {sy116, bzhou}@ie.cuhk.edu.hk

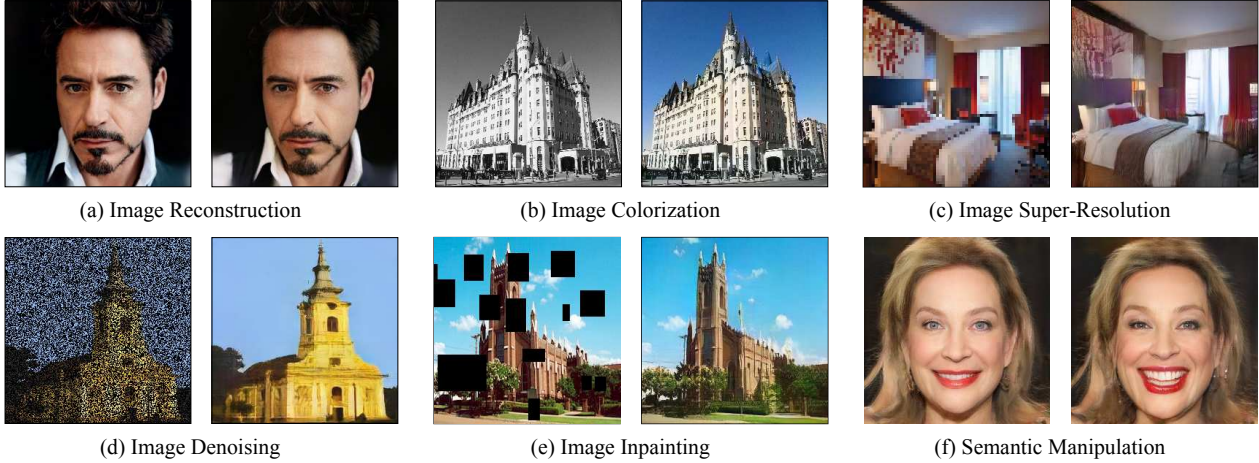


Figure 1: Multi-code GAN prior facilitates many image processing applications using the reconstruction from *fixed* PGGAN [23] models.

## Abstract

Despite the success of Generative Adversarial Networks (GANs) in image synthesis, applying trained GAN models to real image processing remains challenging. Because the generator in GANs typically maps the latent space to the image space, there leaves no space for it to take a real image as the input. To make a trained GAN handle real images, existing methods attempt to invert a target image back to the latent space either by back-propagation or by learning an additional encoder. However, the reconstructions from both of the methods are far from ideal. In this work, we propose a new inversion approach to incorporate the well-trained GANs as effective prior to a variety of image processing tasks. In particular, to invert a given GAN model, we employ multiple latent codes to generate multiple feature maps at some intermediate layer of the generator, then compose them with adaptive channel importance to output the final image. Such an over-parameterization of the latent space significantly improves the image reconstruction quality, outperforming existing GAN inversion methods. The resulting high-fidelity image reconstruction enables the trained GAN models as prior to many real-world applications, such as image colorization, super-resolution, image inpainting, and semantic manipulation. We further analyze the properties of the layer-wise representation learned by

GAN models and shed light on what knowledge each layer is capable of representing.<sup>1</sup>

## 1. Introduction

In recent years, Generative Adversarial Networks (GANs) [16] have significantly advanced image generation by improving the synthesis quality [23, 8, 24] and stabilizing the training process [1, 7, 17]. The capability to produce high-quality images makes GAN applicable to many image processing tasks, such as semantic face editing [27, 35], super-resolution [28, 41], image-to-image translation [51, 11, 31], etc. However, most of these GAN-based approaches require special design of network structures [27, 51] or loss functions [35, 28] for a particular task, making them difficult to generalize to other applications. On the other hand, the large-scale GAN models, like StyleGAN [24] and BigGAN [8], can synthesize photo-realistic images after being trained with millions of diverse images. Their neural representations are shown to contain various levels of semantics underlying the observed data [21, 15, 34, 42]. Reusing these models as prior to real image processing with minor effort could potentially lead to wider applications but remains much less explored.

<sup>1</sup>Code will be made available at [this link](#).

The main challenge towards this goal is that the standard GAN model is initially designed for synthesizing images from random noises, thus is unable to take real images for any post-processing. A common practice is to invert a given image back to a latent code such that it can be reconstructed by the generator. In this way, the inverted code can be used for further processing. To reverse the generation process, there are two existing approaches. One is to directly optimize the latent code by minimizing the reconstruction error through back-propagation [30, 12, 32]. The other is to train an extra encoder to learn the mapping from the image space to the latent space [33, 50, 6, 5]. However, the reconstructions achieved by both methods are far from ideal, especially when the given image is with high resolution. Consequently, the reconstructed image with low quality is unable to be used for image processing tasks.

In principle, it is impossible to recover every detail of any arbitrary real image using a single latent code, otherwise, we would have an unbeatable image compression method. In other words, the expressiveness of using a single latent code is limited by the finite code dimensionality. Therefore, to faithfully reconstruct the given real image, we propose to employ *multiple* latent codes and compose their corresponding feature maps at some intermediate layer of the generator. Utilizing multiple latent codes allows the generator to recover the target image using all the possible composition knowledge learned in the deep generative representations. The experiments show that our approach significantly improves the image reconstruction quality. More importantly, being able to faithfully reconstruct the input image, our approach facilitates various real image processing applications by using pre-trained GAN models as prior *without* retraining or modification, which is shown in Fig. 1.

We summarize our contributions as follows:

- We propose an effective GAN inversion method by using multiple latent codes and adaptive channel importance. The method faithfully reconstructs the given real image, surpassing existing methods.
- We apply the inverted results as the multi-code GAN prior to a range of real-world applications, such as image colorization, super-resolution, image inpainting, semantic manipulation, *etc.*, demonstrating its potential in real image processing.
- We further analyze the importance of the internal representations of different layers in a GAN generator by composing the features from the inverted latent codes at each layer respectively.

## 2. Related Work

**GAN Inversion.** The task of GAN inversion targets at reversing a given image back to a latent code with a pre-trained GAN model. As an important step for applying

GANs to real-world applications, it has attracted increasing attention recently. To invert a fixed generator in GAN, existing methods either optimized the latent code based on gradient descent [30, 12, 32] or learned an extra encoder to project the image space back to the latent space [33, 50, 6, 5]. Bau *et al.* [3] proposed to use encoder to provide better initialization for optimization. There are also some models taking invertibility into account at the training stage [14, 13, 26]. However, all the above methods only consider using a single latent code to recover the input image and the reconstruction quality is far from ideal, especially when the test image shows a huge domain gap to training data. That is because the input image may not lie in the synthesis space of the generator, in which case the perfect inversion with a single latent code does not exist. By contrast, we propose to increase the number of latent codes, which significantly improve the inversion quality no matter whether the target image is in-domain or out-of-domain.

**Image Processing with GANs.** GANs have been widely used for real image processing due to its great power of synthesizing photo-realistic images. These applications include image denoising [9, 25], image inpainting [43, 45], super-resolution [28, 41], image colorization [37, 20], style mixing [19, 10], semantic image manipulation [40, 29], *etc.* However, current GAN-based models are usually designed for a particular task with specialized architectures [19, 40] or loss functions [28, 10], and trained with paired data by taking one image as input and the other as supervision [43, 20]. Differently, our approach can reuse the knowledge contained in a well-trained GAN model and further enable a single GAN model as prior to all the aforementioned tasks *without* retraining or modification. It is worth noticing that our method can achieve similar or even better results than existing GAN-based methods that are particularly trained for a certain task.

**Deep Model Prior.** Generally, the impressive performance of the deep convolutional model can be attributed to its capacity of capturing statistical information from large-scale data as prior. Such prior can be inversely used for image generation and image reconstruction [39, 38, 2]. Upchurch *et al.* [39] inverted a discriminative model, starting from deep convolutional features, to achieve semantic image transformation. Ulyanov *et al.* [38] reconstructed the target image with a U-Net structure to show that the structure of a generator network is sufficient to capture the low-level image statistics prior to any learning. Athar *et al.* [2] learned a universal image prior for a variety of image restoration tasks. Some work theoretically explored the prior provided by deep generative models [32, 18], but the results using GAN prior to real image processing are still unsatisfying. A recent work [3] applied generative image prior to semantic photo manipulation, but it can only edit some partial regions of the input image yet fails to apply

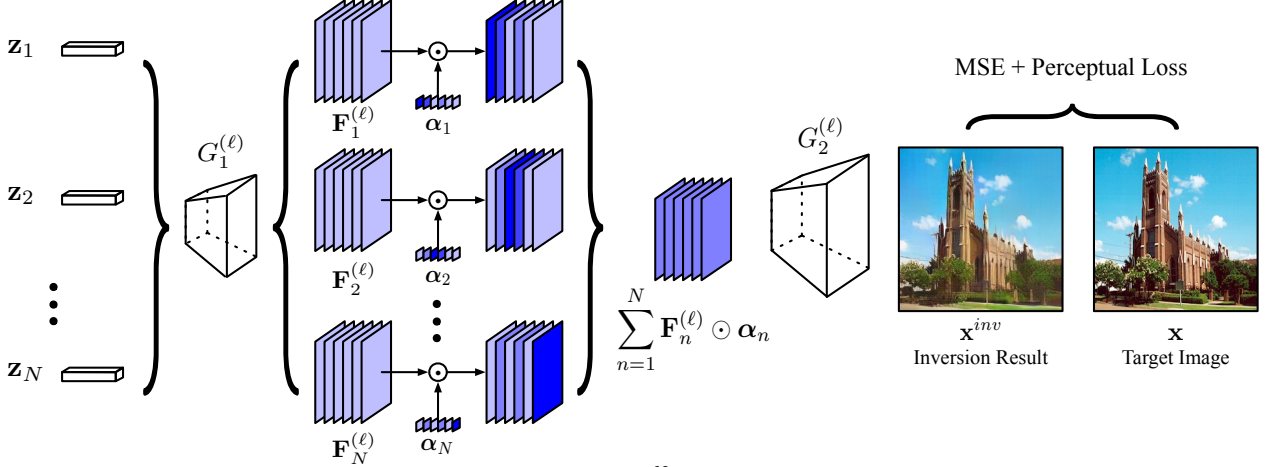


Figure 2: Pipeline of GAN inversion using multiple latent codes  $\{z_n\}_{n=1}^N$ . The generative features from these latent codes are composed at some intermediate layer (*i.e.*, the  $\ell$ -th layer) of the generator, weighted by the adaptive channel importance scores  $\{\alpha_n\}_{n=1}^N$ . All latent codes and the corresponding channel importance scores are jointly optimized to recover a target image.

to other tasks like colorization or super-resolution. That is because it only inverts the GAN model to some intermediate feature space instead of the earliest hidden space. By contrast, our method reverses the entire generative process, *i.e.*, from the image space to the initial latent space, which supports more flexible image processing tasks.

### 3. Multi-Code GAN Prior

A well-trained generator  $G(\cdot)$  of GAN can synthesize high-quality images by sampling codes from the latent space  $\mathcal{Z}$ . Given a target image  $\mathbf{x}$ , the GAN inversion task aims at reversing the generation process by finding the adequate code to recover  $\mathbf{x}$ . It can be formulated as

$$\mathbf{z}^* = \arg \min_{\mathbf{z} \in \mathcal{Z}} \mathcal{L}(G(\mathbf{z}), \mathbf{x}), \quad (1)$$

where  $\mathcal{L}(\cdot, \cdot)$  denotes the objective function.

However, due to the highly non-convex natural of this optimization problem, previous methods fail to ideally reconstruct an arbitrary image by optimizing a single latent code. To this end, we propose to use multiple latent codes and compose their corresponding intermediate feature maps with adaptive channel importance, as illustrated in Fig. 2.

#### 3.1. GAN Inversion with Multiple Latent Codes

The expressiveness of a single latent code may not be enough to recover all the details of a certain image. Then, how about using  $N$  latent codes  $\{z_n\}_{n=1}^N$ , each of which can help reconstruct some sub-regions of the target image? In the following, we introduce how to utilize multiple latent codes for GAN inversion.

**Feature Composition.** One key difficulty after introducing multiple latent codes is how to integrate them in the generation process. A straightforward solution is to fuse

the images generated by each  $z_n$  from the image space  $\mathcal{X}$ . However,  $\mathcal{X}$  is not naturally a linear space such that linearly combining synthesized images is not guaranteed to produce a meaningful image, let alone recover the input in detail. A recent work [5] pointed out that inverting a generative model from the image space to some intermediate feature space is much easier than to the latent space. Accordingly, we propose to combine the latent codes by composing their intermediate feature maps. More concretely, the generator  $G(\cdot)$  is divided into two sub-networks, *i.e.*,  $G_1^{(\ell)}(\cdot)$  and  $G_2^{(\ell)}(\cdot)$ . Here,  $\ell$  is the index of the intermediate layer to perform feature composition. With such a separation, for any  $z_n$ , we can extract the corresponding spatial feature  $\mathbf{F}_n^{(\ell)} = G_1^{(\ell)}(z_n)$  for further composition.

**Adaptive Channel Importance.** Recall that we would like each  $z_n$  to recover some particular regions of the target image. Bau *et al.* [4] observed that different units (*i.e.*, channels) of the generator in GAN are responsible for generating different visual concepts such as objects and textures. Based on this observation, we introduce the adaptive channel importance  $\alpha_n$  for each  $z_n$  to help them align with different semantics. Here,  $\alpha_n \in \mathbb{R}^C$  is a  $C$ -dimensional vector and  $C$  is the number of channels in the  $\ell$ -th layer of  $G(\cdot)$ . We expect each entry of  $\alpha_n$  to represent how important the corresponding channel of the feature map  $\mathbf{F}_n^{(\ell)}$  is. With such composition, the reconstructed image can be generated with

$$\mathbf{x}^{inv} = G_2^{(\ell)}\left(\sum_{n=1}^N \mathbf{F}_n^{(\ell)} \odot \alpha_n\right), \quad (2)$$

where  $\odot$  denotes the channel-wise multiplication as

$$\{\mathbf{F}_n^{(\ell)} \odot \alpha_n\}_{i,j,c} = \{\mathbf{F}_n^{(\ell)}\}_{i,j,c} \times \{\alpha_n\}_c. \quad (3)$$

Here,  $i$  and  $j$  indicate the spatial location, while  $c$  stands for the channel index.

**Optimization Objective.** After introducing the feature composition technique together with the introduced adaptive channel importance to integrate multiple latent codes, there are  $2N$  sets of parameters to be optimized in total. Accordingly we reformulate Eq.(1) as

$$\{\mathbf{z}_n^*\}_{n=1}^N, \{\alpha_n^*\}_{n=1}^N = \arg \min_{\{\mathbf{z}_n\}_{n=1}^N, \{\alpha_n\}_{n=1}^N} \mathcal{L}(\mathbf{x}^{inv}, \mathbf{x}). \quad (4)$$

To improve the reconstruction quality, we define the objective function by leveraging both low-level and high-level information. In particular, we use pixel-wise reconstruction error as well as the  $l_1$  distance between the perceptual features [22] extracted from the two images<sup>2</sup>. Therefore, the objective function is as follows:

$$\mathcal{L}(\mathbf{x}_1, \mathbf{x}_2) = \|\mathbf{x}_1 - \mathbf{x}_2\|_2^2 + \|\phi(\mathbf{x}_1), \phi(\mathbf{x}_2)\|_1, \quad (5)$$

where  $\phi(\cdot)$  denotes the perceptual feature extractor. We use the gradient descent algorithm to find the optimal latent codes as well as the corresponding channel importance scores.

### 3.2. Multi-Code GAN Prior for Image Processing

After inversion, we apply the reconstruction result as the multi-code GAN prior to a variety of image processing tasks. Each task requires an image as a reference, which is the input image for processing. For example, image colorization task deals with grayscale images and image inpainting task restores images with missing holes. Given an input, we apply the proposed multi-code GAN inversion method to reconstruct it and then post-process the reconstructed image to approximate the input. When the approximation is close enough to the input, we assume the reconstruction before post-processing is what we want. Here, to adapt multi-code GAN prior to a specific task, we modify Eq.(5) based on the post-processing function:

- For image colorization task, with a grayscale image  $I_{gray}$  as the input, we expect the inversion result to have the same gray channel as  $I_{gray}$  with

$$\mathcal{L}_{color} = \mathcal{L}(gray(\mathbf{x}^{inv}), I_{gray}), \quad (6)$$

where  $gray(\cdot)$  stands for the operation to take the gray channel of an image.

- For image super-resolution task, with a low-resolution image  $I_{LR}$  as the input, we downsample the inversion result to approximate  $I_{LR}$  with

$$\mathcal{L}_{SR} = \mathcal{L}(down(\mathbf{x}^{inv}), I_{LR}), \quad (7)$$

where  $down(\cdot)$  stands for the downsampling operation.

<sup>2</sup>In this experiment, we use pre-trained VGG-16 model [36] as the feature extractor, and the output of layer conv\_43 is used.

- For image inpainting task, with an intact image  $I_{ori}$  and a binary mask  $\mathbf{m}$  indicating known pixels, we only reconstruct the incorrupt parts and let the GAN model fill in the missing pixels automatically with

$$\mathcal{L}_{inp} = \mathcal{L}(\mathbf{x}^{inv} \circ \mathbf{m}, I_{ori} \circ \mathbf{m}), \quad (8)$$

where  $\circ$  denotes the element-wise product.

## 4. Experiments

We conduct extensive experiments on state-of-the-art GAN models, *i.e.*, PGGAN [23] and StyleGAN [24], to verify the effectiveness of the multi-code GAN prior. These models are trained on various datasets, including CelebA-HQ [23] and FFHQ [24] for faces as well as LSUN [44] for scenes. We first compare our approach with existing GAN inversion methods in Sec.4.1. We then apply our approach to a variety of image processing tasks in Sec.4.2 to show that trained GAN models can be used as prior to various real-world applications. We finally analyze the per-layer representation learned by GANs in Sec.4.3. The ablation study on the proposed method can be found in **Appendix**.

### 4.1. Comparison with Other Inversion Methods

There are many attempts on GAN inversion in the literature. In this section, we compare our multi-code inversion approach with the following baseline methods: (a) optimizing a single latent code  $\mathbf{z}$  as in Eq.(1) [32], (b) learning an encoder to reverse the generator [50], and (c) combining (a) and (b) by using the output of the encoder as the initialization for further optimization [5].

To quantitatively evaluate the inversion results, we introduce the Peak Signal-to-Noise Ratio (PSNR) to measure the similarity between the original input and the reconstruction result from pixel level, as well as the LPIPS metric [47] which is known to align with human perception. We make comparisons on three PGGAN [23] models that are trained on LSUN bedroom (indoor scene), LSUN church (outdoor scene), and CelebA-HQ (human face) respectively. For each model, we invert 300 real images for testing.

Tab.1 and Fig.3 show the quantitative and qualitative comparisons respectively. From Tab.1, we can tell that our

Table 1: Quantitative comparison of different GAN inversion methods: including (a) optimizing a single latent code [30, 32], (b) learning an encoder [50], (c) using the encoder as initialization for optimization [5], and (d) our proposed multi-code GAN prior.  $\uparrow$  means the higher the better while  $\downarrow$  means the lower the better.

Method	Bedroom		Church		Face	
	PSNR $\uparrow$	LPIPS $\downarrow$	PSNR $\uparrow$	LPIPS $\downarrow$	PSNR $\uparrow$	LPIPS $\downarrow$
(a)	17.19	0.5897	17.15	0.5339	19.17	0.5797
(b)	11.59	0.6247	11.58	0.5961	11.18	0.6992
(c)	18.34	0.5201	17.81	0.4789	20.33	0.5321
(d)	<b>25.13</b>	<b>0.1578</b>	<b>22.76</b>	<b>0.1799</b>	<b>23.59</b>	<b>0.4432</b>



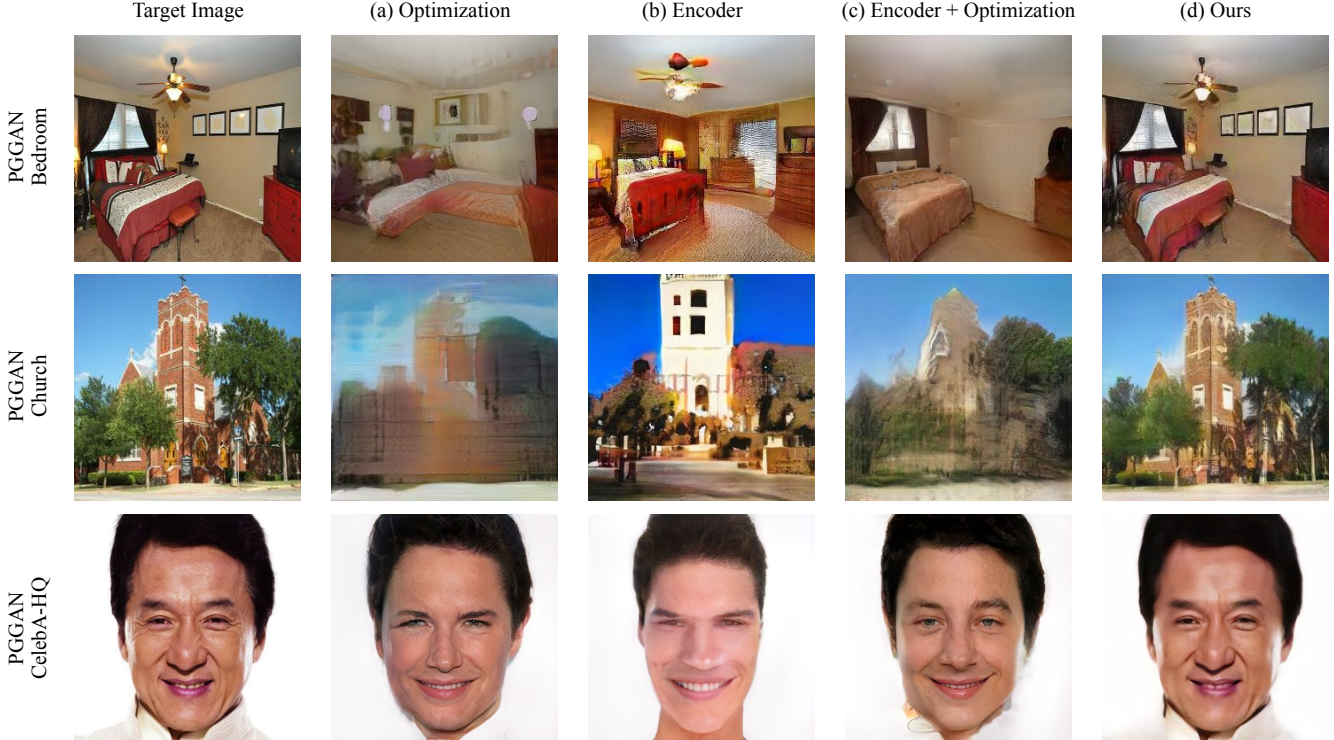


Figure 3: Qualitative comparison of different GAN inversion methods, including (a) optimizing a single latent code [30, 32], (b) learning an encoder [50], (c) using the encoder as initialization for optimization [5], and (d) our proposed multi-code GAN prior.

multi-code inversion beats other competitors on all three models from both pixel level (PSNR) and perception level (LPIPS). We also observe in Fig.3 that existing methods fail to recover the details of the target image, which is due to the limited representation capability of a single latent code. By contrast, our method achieves much more satisfying reconstructions with most details, benefiting from multiple latent codes. We even recover an eastern face with a model trained on western data (CelebA-HQ [23]).

## 4.2. Image Processing Applications

With the high-fidelity image reconstruction, our multi-code inversion method facilitates many image processing tasks with *pre-trained* GANs as prior. In this section, we apply our method to a variety of real-world applications to demonstrate its effectiveness, including image colorization, image super-resolution, image inpainting and denoising, as well as semantic manipulation and style mixing. For each application, the GAN model is *fixed* without retraining.

**Image Colorization.** Given a grayscale image as input, we can colorize it with the proposed multi-code GAN prior as described in Sec.3.2. We compare our inversion method with optimizing the intermediate feature maps [3]. We also compare with DIP [38], which uses a discriminative model as prior, and Zhang *et al.* [46], which is specially designed for colorization task. We do experiments on PGGAN models trained for bedroom and church synthesis,

Table 2: Quantitative evaluation results on colorization task with bedroom and church images. AuC refers to the area under the curve of the cumulative error distribution over *ab* color space [46].  $\uparrow$  means higher score is better.

Method	Bedroom AuC (%) $\uparrow$	Church AuC (%) $\uparrow$
Grayscale input	88.02	85.50
(a) Optimizing feature maps [3]	85.41	86.10
(b) DIP [38]	84.33	83.31
(c) Zhang <i>et al.</i> [46]	88.55	89.13
(d) Ours	<b>90.02</b>	<b>89.43</b>

and use the area under the curve of the cumulative error distribution over *ab* color space as the evaluation metric, following [46]. Tab.2 and Fig.4 show the quantitative and qualitative comparisons respectively. It turns out that using the discriminative model as prior fails to colorize the image adequately. That is because discriminative models focus on learning high-level representations and hence perform badly in low-level tasks. On the contrary, using the generative model as prior leads to much more satisfying colorful images. We also achieve comparable results as the model whose primary goal is image colorization (Fig.4 (c) and (d)). This benefits from the rich knowledge GANs have learned when trained to synthesize photo-realistic images. Note that Zhang *et al.* [46] is proposed for general image colorization, while our approach can be only applied to a certain image category corresponding to the given GAN model. A larger GAN model trained on a more diverse dataset should improve its generalization ability.

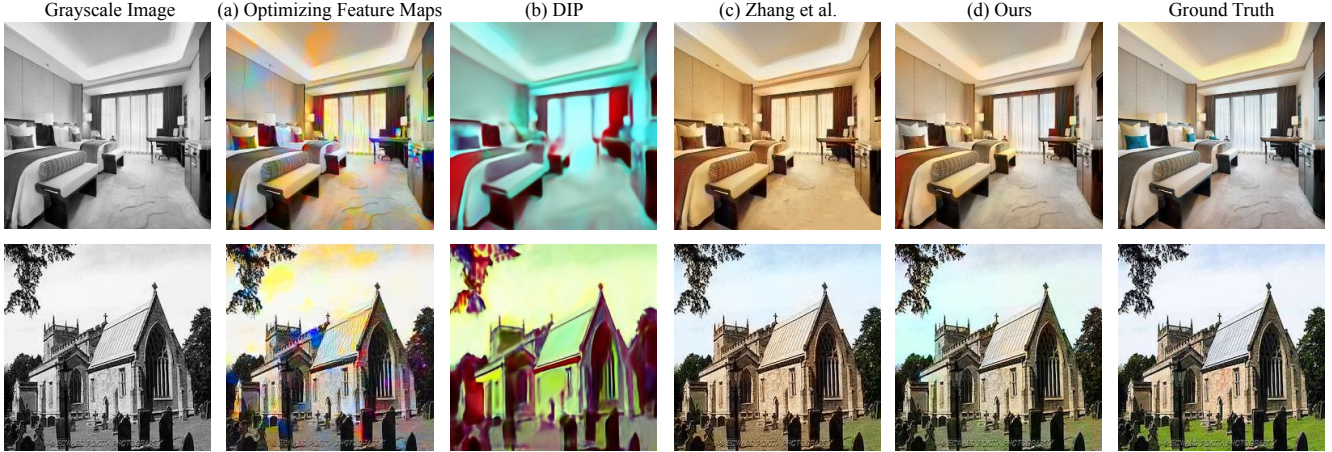


Figure 4: Qualitative comparison of different colorization methods, including (a) inversion by optimizing feature maps [3], (b) DIP [38], (c) Zhang *et al.* [46], and (d) our proposed multi-code GAN prior.

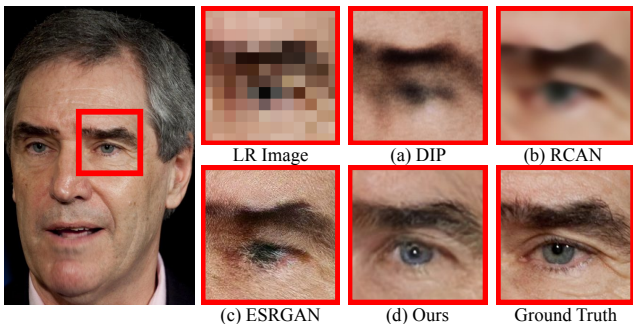


Figure 5: Qualitative comparison of different super-resolution methods with SR factor 16. Competitors include DIP [38], RCAN [48], and ESRGAN [41].

**Image Super-Resolution.** We also evaluate our approach on the image super-resolution (SR) task. We do experiments on the PGGAN model trained for face synthesis and set the SR factor as 16. Such a large factor is very challenging for the SR task. We compare with DIP [38] as well as the state-of-the-art SR methods, RCAN [48] and ESRGAN [41]. Besides PSNR and LPIPS, we introduce Naturalness Image Quality Evaluator (NIQE) as an extra metric. Tab.3 shows the quantitative comparison. We can conclude that our approach achieves comparable or even better performance than the advanced learning-based competitors. A visualization example is also shown in Fig.5, where our method reconstructs the human eye with more details. Compared to existing learning-based models, like RCAN and ESRGAN, our multi-code GAN prior is more flexible to the SR factor. This suggests that the freely-trained PGGAN model has spontaneously learned rich knowledge such that it can be used as prior to enhance a low-resolution (LR) image.

**Image Inpainting and Denoising.** We further extend our approach to image restoration tasks, like image inpainting and image denoising. We first corrupt the image contents by randomly cropping or adding noises, and then use different algorithms to restore them. Experiments are conducted

Table 3: Quantitative comparison of different super-resolution methods with SR factor 16. Competitors include DIP [38], RCAN [48], and ESRGAN [41].  $\uparrow$  means the higher the better while  $\downarrow$  means the lower the better.

Method	PSNR $\uparrow$	LPIPS $\downarrow$	NIQE $\downarrow$
(a) DIP [38]	26.87	0.4236	4.66
(b) RCAN [48]	<b>28.82</b>	0.4579	5.70
(c) ESRGAN [41]	25.26	0.3862	3.27
(d) Ours	26.93	<b>0.3584</b>	<b>3.19</b>

Table 4: Quantitative comparison of different inpainting methods. We do test with both centrally cropping a  $64 \times 64$  box and randomly cropping 80% pixels.  $\uparrow$  means higher score is better.

Method	Center Crop		Random Crop	
	PSNR $\uparrow$	SSIM $\uparrow$	PSNR $\uparrow$	SSIM $\uparrow$
(a) Single latent code [30, 32]	10.37	0.1672	12.79	0.1783
(b) Optimizing feature maps [3]	14.75	0.4563	18.72	0.2793
(c) DIP [38]	17.92	0.4327	18.02	0.2823
(d) Ours	<b>21.43</b>	<b>0.5320</b>	<b>22.11</b>	<b>0.5532</b>

on PGGAN models and we compare with several baseline inversion methods as well as DIP [38]. PSNR and Structural SIMilarity (SSIM) are used as evaluation metrics. Tab.4 shows the quantitative comparison, where our approach achieves the best performances on both settings of center crop and random crop. Fig.6 includes some examples of restoring corrupted images. It is obvious that both existing inversion methods and DIP fail to adequately fill in the missing pixels or completely remove the added noises. By contrast, our method is able to use multi-code GAN prior to convincingly repair the corrupted images with meaningful filled content.

**Semantic Manipulation and Style Mixing.** Besides the aforementioned low-level applications, we also test our approach with some high-level tasks, like semantic manipulation and style mixing. As pointed out by prior work [21, 15, 34], GANs have already encoded some interpretable semantics inside the latent space. From this point, our inversion method provides a feasible way to





Figure 6: Qualitative comparison of different inpainting methods, including (a) inversion by optimizing a single latent code [30, 32], (b) inversion by optimizing feature maps [3], (c) DIP [38], and (d) our multi-code GAN prior.

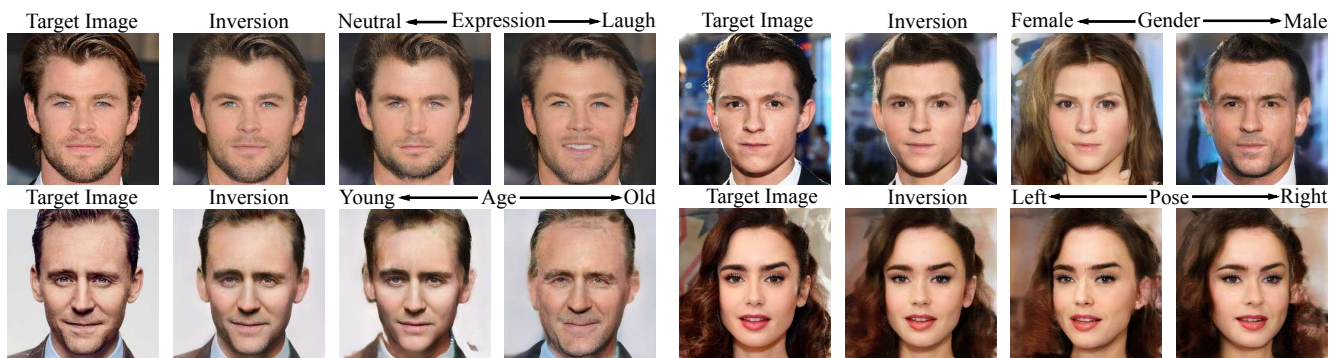


Figure 7: Real face manipulation with respect to four various attributes. In each four-element tuple, from left to right are: input face, inversion result, and manipulation results by making a particular semantic more negative and more positive.

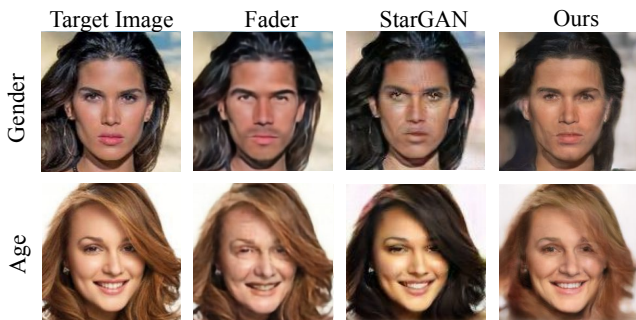


Figure 8: Qualitative comparison of different real face manipulation methods, including Fader [27], StarGAN [11], and our proposed multi-code GAN prior. Note that we achieve competitive results *without* redesigning the network or retraining the model. Also, our approach enables the high-resolution manipulation with image size  $1024 \times 1024$ . Zoom in for details.

utilize these learned semantics for *real* image manipulation. We apply the manipulation framework based on latent code proposed in [34] to achieve semantic facial attribute editing. Fig.7 shows the manipulation results and Fig.8 compares our multi-code GAN prior with some ad hoc models designed for face manipulation, *i.e.*, Fader [27] and StarGAN [11]. We see that the GAN prior can provide rich enough information for semantic manipulation, achieving competitive results. We also conduct experiments on the StyleGAN [24] model to show the reconstruction from the multi-code GAN inversion supports style mixing. As shown in Fig.9, we successfully exchange styles from different levels between source and target images, suggesting that our inversion method can well recover the input image with respect to different levels of semantics.

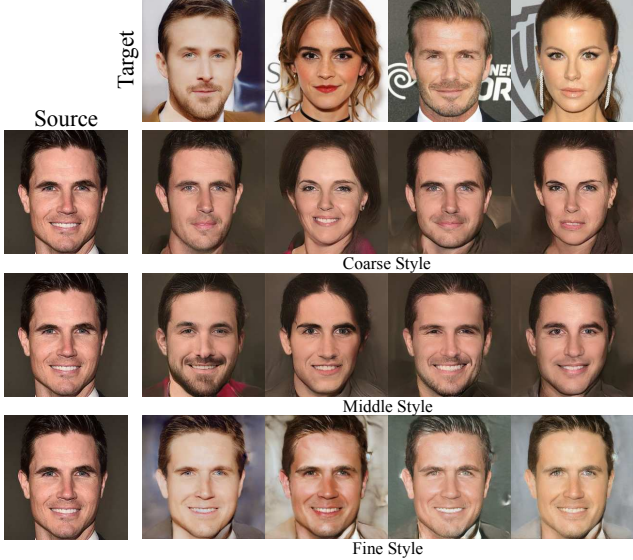


Figure 9: Style mixing results on real faces with StyleGAN [24] model as prior. We first invert both the source image and the target images. Then we copy the style codes from reconstructed target images to those from the source image at different levels, *i.e.*, coarse-level (low-level), middle-level, and fine-level (high-level).

### 4.3. Knowledge Representation in GANs

As discussed above, one key reason for single latent code failing to invert the input image is its limited expressiveness, especially when the test image contains contents different to the training data. Here we verify whether the proposed multi-code GAN inversion is able to reuse the GAN knowledge learned for a domain to reconstruct an image from a different domain. In particular, we try to use GAN models trained for synthesizing face, church, conference room, and bedroom, to invert a bedroom image. As shown in Fig. 10, when using a single latent code, the reconstructed image still lies in the original training domain (*e.g.*, the inversion with PGGAN CelebA-HQ model looks like a face instead of a bedroom). On the contrary, our multi-code method is able to compose a bedroom image no matter what kind of images the GAN generator is trained with.

We further analyze the layer-wise knowledge of a well-trained GAN model by performing feature composition at different layers. The result is included in Fig. 10. It turns out that the higher layer is used, the better the reconstruction will be. That is because reconstruction focuses on recovering low-level pixel values, and GANs tend to represent abstract semantics at bottom-intermediate layers while representing content details at top layers. We also observe that the 4th layer is good enough for the bedroom model to invert a bedroom image, but the other three models need the 8th layer for satisfying inversion. The reason is that bedroom shares different semantics from face, church, and conference room. Hence, such high-level

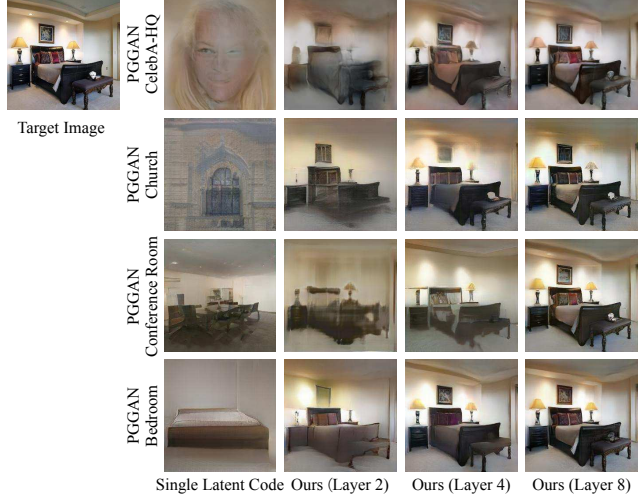


Figure 10: Comparison of the inversion results using different GAN models as well as performing feature composition at different layers. Each row stands for a PGGAN model trained on a specific dataset as prior, while each column shows results by composing feature maps at a certain layer.

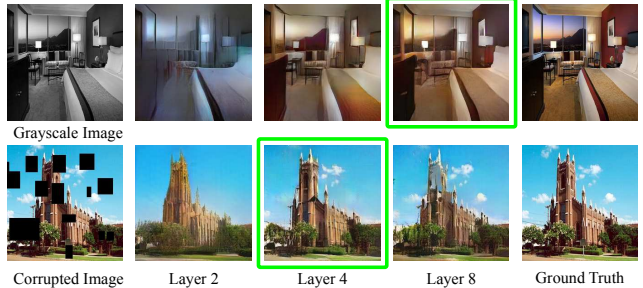


Figure 11: Colorization and inpainting results with multi-code GAN prior using different composition layers. AuC (the higher the better) for colorization task are 86.83%, 87.44%, 90.02% with respect to the 2nd, 4th, and 8th layer respectively. PSNR (the higher the better) for inpainting task are 21.19db, 22.11db, 20.70db with respect to the 2nd, 4th, and 8th layer respectively. Images in green boxes indicate the best results.

knowledge from these models cannot be reused. We further make per-layer analysis by applying our approach to image colorization and image inpainting tasks, as shown in Fig. 11. The colorization task gets the best result at the 8th layer while the inpainting task at the 4th layer. That is because colorization is more like a low-level rendering task while inpainting requires the GAN prior to fill in the missing content with meaningful objects. This is consistent with the analysis from Fig. 10, which is that low-level knowledge from GAN prior can be reused at higher layers while high-level knowledge at lower layers.

## 5. Conclusion

We present a novel GAN inversion method that employs multiple latent codes for reconstructing real images with a pre-trained GAN model. Extensive experimental results



suggest that the pre-trained GAN equipped with our inversion method can be used as a very powerful image prior for a variety of image processing tasks.

## References

- [1] Martin Arjovsky, Soumith Chintala, and Léon Bottou. Wasserstein gan. *arXiv preprint arXiv:1701.07875*, 2017. **1**
- [2] ShahRukh Athar, Evgeny Burnaev, and Victor Lempitsky. Latent convolutional models. In *ICLR*, 2019. **2**
- [3] David Bau, Hendrik Strobelt, William Peebles, Jonas Wulff, Bolei Zhou, Jun-Yan Zhu, and Antonio Torralba. Semantic photo manipulation with a generative image prior. *SIGGRAPH*, 2019. **2, 5, 6, 7**
- [4] David Bau, Jun-Yan Zhu, Hendrik Strobelt, Bolei Zhou, Joshua B. Tenenbaum, William T. Freeman, and Antonio Torralba. Gan dissection: Visualizing and understanding generative adversarial networks. In *ICLR*, 2019. **3, 10, 12**
- [5] David Bau, Jun-Yan Zhu, Jonas Wulff, William Peebles, Hendrik Strobelt, Bolei Zhou, and Antonio Torralba. Inverting layers of a large generator. In *ICLR Workshop*, 2019. **2, 3, 4, 5**
- [6] David Bau, Jun-Yan Zhu, Jonas Wulff, William Peebles, Hendrik Strobelt, Bolei Zhou, and Antonio Torralba. Seeing what a gan cannot generate. In *ICCV*, 2019. **2**
- [7] David Berthelot, Thomas Schumm, and Luke Metz. Began: Boundary equilibrium generative adversarial networks. *arXiv preprint arXiv:1703.10717*, 2017. **1**
- [8] Andrew Brock, Jeff Donahue, and Karen Simonyan. Large scale gan training for high fidelity natural image synthesis. *ICLR*, 2019. **1**
- [9] Jingwen Chen, Jiawei Chen, Hongyang Chao, and Ming Yang. Image blind denoising with generative adversarial network based noise modeling. In *CVPR*, 2018. **2**
- [10] Xinyuan Chen, Chang Xu, Xiaokang Yang, Li Song, and Dacheng Tao. Gated-gan: Adversarial gated networks for multi-collection style transfer. *TIP*, 2018. **2**
- [11] Yunjey Choi, Minje Choi, Munyoung Kim, Jung-Woo Ha, Sunghun Kim, and Jaegul Choo. Stargan: Unified generative adversarial networks for multi-domain image-to-image translation. In *CVPR*, 2018. **1, 7**
- [12] Antonia Creswell and Anil Anthony Bharath. Inverting the generator of a generative adversarial network. *TNNLS*, 2018. **2**
- [13] Jeff Donahue, Philipp Krähenbühl, and Trevor Darrell. Adversarial feature learning. In *ICLR*, 2017. **2**
- [14] Vincent Dumoulin, Ishmael Belghazi, Ben Poole, Olivier Mastropietro, Alex Lamb, Martin Arjovsky, and Aaron Courville. Adversarially learned inference. In *ICLR*, 2017. **2**
- [15] Lore Goetschalckx, Alex Andonian, Aude Oliva, and Phillip Isola. Ganalyze: Toward visual definitions of cognitive image properties. In *ICCV*, 2019. **1, 6**
- [16] Ian Goodfellow, Jean Pouget-Abadie, Mehdi Mirza, Bing Xu, David Warde-Farley, Sherjil Ozair, Aaron Courville, and Yoshua Bengio. Generative adversarial nets. In *NeurIPS*, 2014. **1**
- [17] Ishaan Gulrajani, Faruk Ahmed, Martin Arjovsky, Vincent Dumoulin, and Aaron C Courville. Improved training of wasserstein gans. In *NeurIPS*, 2017. **1**
- [18] Paul Hand and Vladislav Voroninski. Global guarantees for enforcing deep generative priors by empirical risk. *IEEE Transactions on Information Theory*, 2019. **2**
- [19] Guang-Yuan Hao, Hong-Xing Yu, and Wei-Shi Zheng. Mix-gan: learning concepts from different domains for mixture generation. In *IJCAI*, 2018. **2**
- [20] Phillip Isola, Jun-Yan Zhu, Tinghui Zhou, and Alexei A Efros. Image-to-image translation with conditional adversarial networks. In *CVPR*, 2017. **2**
- [21] Ali Jahanian, Lucy Chai, and Phillip Isola. On the “steerability” of generative adversarial networks. *arXiv preprint arXiv:1907.07171*, 2019. **1, 6**
- [22] Justin Johnson, Alexandre Alahi, and Li Fei-Fei. Perceptual losses for real-time style transfer and super-resolution. In *ECCV*, 2016. **4**
- [23] Tero Karras, Timo Aila, Samuli Laine, and Jaakko Lehtinen. Progressive growing of gans for improved quality, stability, and variation. In *ICLR*, 2018. **1, 4, 5, 10, 13, 14**
- [24] Tero Karras, Samuli Laine, and Timo Aila. A style-based generator architecture for generative adversarial networks. *CVPR*, 2019. **1, 4, 7, 8, 10, 13, 15, 19**
- [25] Dong-Wook Kim, Jae Ryun Chung, and Seung-Won Jung. Grdn: Grouped residual dense network for real image denoising and gan-based real-world noise modeling. In *CVPR Workshop*, 2019. **2**
- [26] Durk P Kingma and Prafulla Dhariwal. Glow: Generative flow with invertible 1x1 convolutions. In *NeurIPS*, 2018. **2**
- [27] Guillaume Lample, Neil Zeghidour, Nicolas Usunier, Antoine Bordes, Ludovic Denoyer, and Marc’Aurelio Ranzato. Fader networks: Manipulating images by sliding attributes. In *NeurIPS*, 2017. **1, 7**
- [28] Christian Ledig, Lucas Theis, Ferenc Huszár, Jose Caballero, Andrew Cunningham, Alejandro Acosta, Andrew Aitken, Alykhan Tejani, Johannes Totz, Zehan Wang, et al. Photo-realistic single image super-resolution using a generative adversarial network. In *CVPR*, 2017. **1, 2**
- [29] Xiaodan Liang, Hao Zhang, Liang Lin, and Eric Xing. Generative semantic manipulation with mask-contrasting gan. In *ECCV*, 2018. **2**
- [30] Zachary C Lipton and Subarna Tripathi. Precise recovery of latent vectors from generative adversarial networks. In *ICLR Workshop*, 2017. **2, 4, 5, 6, 7**
- [31] Ming-Yu Liu, Xun Huang, Arun Mallya, Tero Karras, Timo Aila, Jaakko Lehtinen, and Jan Kautz. Few-shot unsupervised image-to-image translation. In *ICCV*, 2019. **1**
- [32] Fangchang Ma, Ulas Ayaz, and Sertac Karaman. Invertibility of convolutional generative networks from partial measurements. In *NeurIPS*, 2018. **2, 4, 5, 6, 7**
- [33] Guim Perarnau, Joost Van De Weijer, Bogdan Raducanu, and Jose M Álvarez. Invertible conditional gans for image editing. In *NeurIPS Workshop*, 2016. **2**
- [34] Yujun Shen, Jinjin Gu, Xiaoou Tang, and Bolei Zhou. Interpreting the latent space of gans for semantic face editing. *arXiv preprint arXiv:1907.10786*, 2019. **1, 6, 7**

- [35] Yujun Shen, Ping Luo, Junjie Yan, Xiaogang Wang, and Xiaoou Tang. Faceid-gan: Learning a symmetry three-player gan for identity-preserving face synthesis. In *CVPR*, 2018. 1
- [36] Karen Simonyan and Andrew Zisserman. Very deep convolutional networks for large-scale image recognition. *ICLR*, 2015. 4
- [37] Patricia L Suárez, Angel D Sappa, and Boris X Vintimilla. Infrared image colorization based on a triplet dcgan architecture. In *CVPR Workshop*, 2017. 2
- [38] Dmitry Ulyanov, Andrea Vedaldi, and Victor Lempitsky. Deep image prior. In *CVPR*, 2018. 2, 5, 6, 7
- [39] Paul Upchurch, Jacob Gardner, Geoff Pleiss, Robert Pless, Noah Snaveley, Kavita Bala, and Kilian Weinberger. Deep feature interpolation for image content changes. In *CVPR*, 2017. 2
- [40] Ting-Chun Wang, Ming-Yu Liu, Jun-Yan Zhu, Andrew Tao, Jan Kautz, and Bryan Catanzaro. High-resolution image synthesis and semantic manipulation with conditional gans. In *CVPR*, 2018. 2
- [41] Xintao Wang, Ke Yu, Shixiang Wu, Jinjin Gu, Yihao Liu, Chao Dong, Yu Qiao, and Chen Change Loy. Esrgan: Enhanced super-resolution generative adversarial networks. In *ECCV Workshop*, 2018. 1, 2, 6, 13, 15
- [42] Ceyuan Yang, Yujun Shen, and Bolei Zhou. Semantic hierarchy emerges in deep generative representations for scene synthesis. *arXiv preprint arXiv:1911.09267*, 2019. 1
- [43] Raymond A Yeh, Chen Chen, Teck Yian Lim, Alexander G Schwing, Mark Hasegawa-Johnson, and Minh N Do. Semantic image inpainting with deep generative models. In *CVPR*, 2017. 2
- [44] Fisher Yu, Ari Seff, Yinda Zhang, Shuran Song, Thomas Funkhouser, and Jianxiong Xiao. Lsun: Construction of a large-scale image dataset using deep learning with humans in the loop. *arXiv preprint arXiv:1506.03365*, 2015. 4
- [45] Jiahui Yu, Zhe Lin, Jimei Yang, Xiaohui Shen, Xin Lu, and Thomas S Huang. Generative image inpainting with contextual attention. In *CVPR*, 2018. 2
- [46] Richard Zhang, Phillip Isola, and Alexei A Efros. Colorful image colorization. In *ECCV*, 2016. 5, 6, 16
- [47] Richard Zhang, Phillip Isola, Alexei A Efros, Eli Shechtman, and Oliver Wang. The unreasonable effectiveness of deep features as a perceptual metric. In *CVPR*, 2018. 4
- [48] Yulun Zhang, Kunpeng Li, Kai Li, Lichen Wang, Bineng Zhong, and Yun Fu. Image super-resolution using very deep residual channel attention networks. In *ECCV*, 2018. 6, 13, 15
- [49] Bolei Zhou, Hang Zhao, Xavier Puig, Sanja Fidler, Adela Barriuso, and Antonio Torralba. Scene parsing through ade20k dataset. In *CVPR*, 2017. 10
- [50] Jun-Yan Zhu, Philipp Krähenbühl, Eli Shechtman, and Alexei A Efros. Generative visual manipulation on the natural image manifold. In *ECCV*, 2016. 2, 4, 5
- [51] Jun-Yan Zhu, Taesung Park, Phillip Isola, and Alexei A Efros. Unpaired image-to-image translation using cycle-consistent adversarial networks. In *ICCV*, 2017. 1

## Appendix

We first show the visualization of the role of each latent code in our multi-code inversion method in Sec.A. We then conduct ablation study in Sec.B. Finally, we provide more inversion results for both PGGAN [23] and StyleGAN [24] in Sec.C, as well as more application results in Sec.D.

### A. Role of Each Latent Code

We use multiple latent codes  $\{\mathbf{z}\}_{n=1}^N$  for inversion by expecting each of them to take charge of inverting a particular region and hence complement with each other. In this part, we visualize the roles that different latent codes play in the inversion process. Specifically, we are interested in how each latent code corresponds to the visual concepts and regions of the target image.

As pointed out by [4], for a particular layer in a GAN model, different units (channels) control different semantic concepts. Recall that we use adaptive channel importance to help determine what kind of semantics a particular  $\mathbf{z}$  should focus on. To reveal such a relationship, we compute the difference map for each latent code, which refers to the changing of the reconstructed image when this latent code is ablated. Here, to ablate a latent code, we do not simply drop it. Instead, by ranking the values of the channel weights, we select the most principal channels (*i.e.*, those with the largest weights), and disable these channels by setting the corresponding weights as zero. In our experiments, we ablate all channels whose importance weights are larger than 0.2 and obtain a difference map  $\mathbf{r}_n$  for each latent code  $\mathbf{z}_n$ .

We further annotate the semantic concept for each latent code, similarly to how the individual filters are annotated in [4]. We first use the segmentation model [49] to segment the generated image into several semantic regions. Then we quantify the spatial agreement between the difference map and the segmentation of a concept  $c$  with the Intersection-over-Union (IoU) measure:

$$\text{IoU}_{\mathbf{z}_n, c} = \frac{(\mathbf{r}'_n > t) \wedge \mathbf{s}_c(\mathbf{x}^{inv})}{(\mathbf{r}'_n > t) \vee \mathbf{s}_c(\mathbf{x}^{inv})}, \quad (9)$$

where  $\wedge$  and  $\vee$  denote intersection and union operation.  $\mathbf{s}_c(\mathbf{x}^{inv})$  denotes the segmentation result of  $\mathbf{x}^{inv}$  to the concept  $c$ .  $\mathbf{r}'_n = (\mathbf{r}_n - \min(\mathbf{r}_n)) / (\max(\mathbf{r}_n) - \min(\mathbf{r}_n))$  is the normalized difference map, and  $t$  is the threshold. We can rank the concepts related to each latent code with  $\text{IoU}_{\mathbf{z}_n, c}$  and label each latent code with the concept that matches best. Fig.12 shows the segmentation result and examples of some latent codes with high  $\text{IoU}_{\mathbf{z}_n, c}$ . It turns out that the latent codes are specialized to invert different meaningful image regions to compose the whole image. This is also a huge advantage of using multiple latent codes over using a single code.



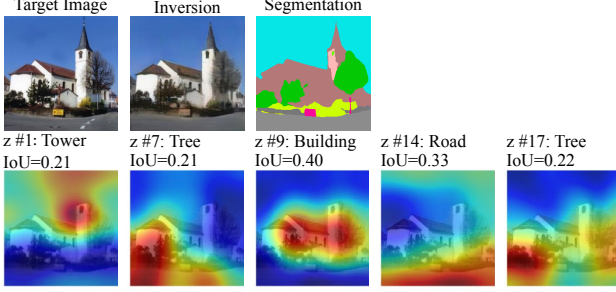


Figure 12: Visualization of the role of each latent code. Images on the top row are the target image, inversion result, and the corresponding segmentation mask, respectively. On the bottom row are several latent codes annotated with a semantic label and the corresponding  $\text{IoU}_{z_n, c}$ .

## B. Ablation Study on Inversion

In this section, we make ablation study on the proposed multi-code GAN inversion method. Compared to existing approaches, we make two major improvements by (i) employing multiple latent codes, and (ii) performing feature composition with adaptive channel importance. Accordingly, we first evaluate how the number of latent codes used affects the inversion results in Sec.B.1. We then explore the effectiveness of proposed adaptive channel importance by comparing it with other feature composition methods in Sec.B.2. Finally, we analyze how composing features at different layers affects the inversion quality in Sec.B.3.

### B.1. Number of Latent Codes

Recall that our method achieves high-fidelity GAN inversion with  $N$  latent codes and  $N$  importance factors. Taking PGGAN as an example, if we choose the 6th layer as the composition layer with  $N = 10$ , the number of parameters to optimize is  $10 \times (512 + 512)$ , which is 20 times the dimension of the original latent space. Despite more parameters used, the recovered results significantly surpass those by optimizing single  $\mathbf{z}$ . Obviously, there is a trade-off between the dimension of optimization space and the inversion quality. To better analysis such trade-off, we evaluate our method by varying the number of latent codes employed. Fig.13 shows that the more latent codes used for inversion, the better inversion result we are able to obtain. However, it does not imply that the inversion results can be infinitely improved by just increasing the number of latent codes. From Fig.13, we can see that after the number reaches 20, there is no significant growth via involving more latent codes.

We have also empirically found that using multiple latent codes also improves optimization stability. Recall that due to the non-convex nature of the optimization problem as well as some cases where the solution does not exist, we can only attempt to find some approximation solution.

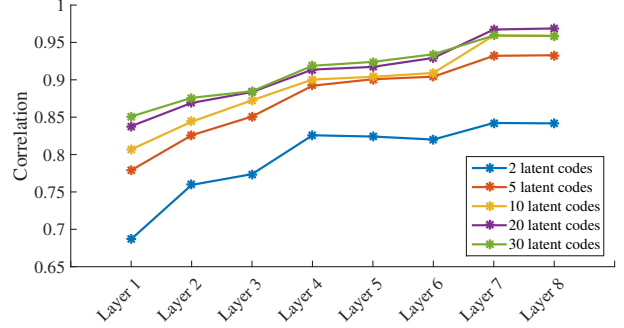


Figure 13: Effects on inversion performance by the feature composition position and the number of latent codes used.

Such a process strongly relies on the initialization such that different initialization points may lead to different local minima. In the case of using only one latent code, the inversion quality varies a lot based on different initialization points, as shown in Fig.14. Here, we randomly initialize the latent code for 20 times, and all of them lead to different results, suggesting that the optimization process is very sensitive to the starting point. On the contrary, the over-parameterization design of using multiple latent codes enhances the stability. For example, for the scene image inversion case, the correlation of the target image and the reconstructed one is  $0.772 \pm 0.071$  for traditional inversion method with a single  $\mathbf{z}$ , and is improved to  $0.927 \pm 0.006$  by introducing multiple latent codes. Accordingly, our method yields high-fidelity inversion results as well as strong stability.

### B.2. Composition Method

In this part, we evaluate the effectiveness of different feature composition methods. Two alternative strategies are compared, including (a) averaging the spatial feature maps with  $\frac{1}{N} \sum_{n=1}^N \mathbf{F}_n^{(\ell)}$ , and (b) weighted-averaging the spatial feature maps without considering the channel discrepancy as  $\frac{1}{N} \sum_{n=1}^N w_n \mathbf{F}_n^{(\ell)}$ . Fig.15 shows the comparison results between different feature composition methods on the PGGAN model trained for synthesizing outdoor church and human face. For the averaging method, it fails to reconstruct even the shape of the target image. For the weighted-averaging method, it manages to assign different importance scores for different latent codes so as to better recover the shape of the target image. However, without channel-wise importance, it also fails to reconstruct the detailed texture, *e.g.*, the tree in the church image in Fig.15. By contrast, our full method successfully reconstructs both the shape and the texture of the target image.

### B.3. Different Composition Layers

On which layer to perform feature composition also affects the performance of the proposed method. To analyze

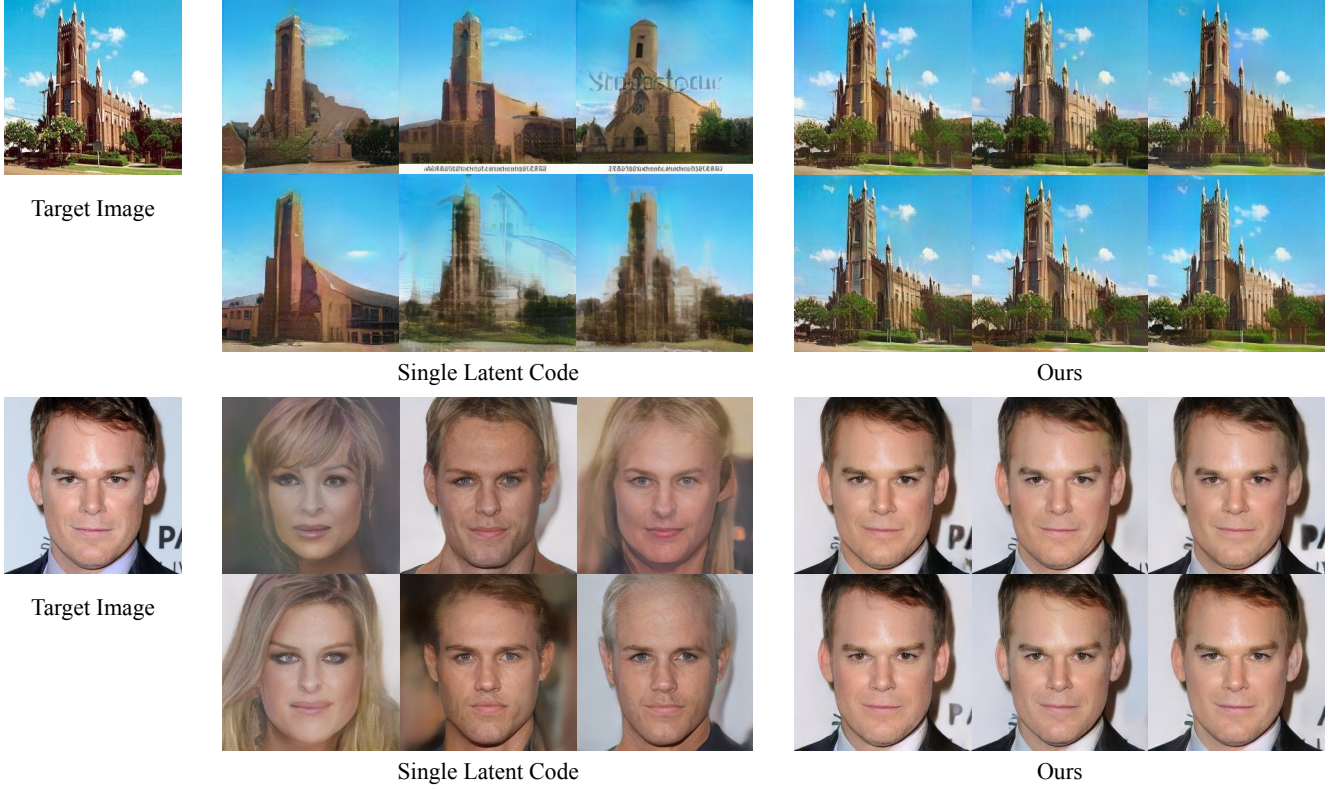


Figure 14: Comparison on how different initialization points will affect the inversion results. Compared to optimizing a single latent code, our multi-code inversion method shows stronger stability.

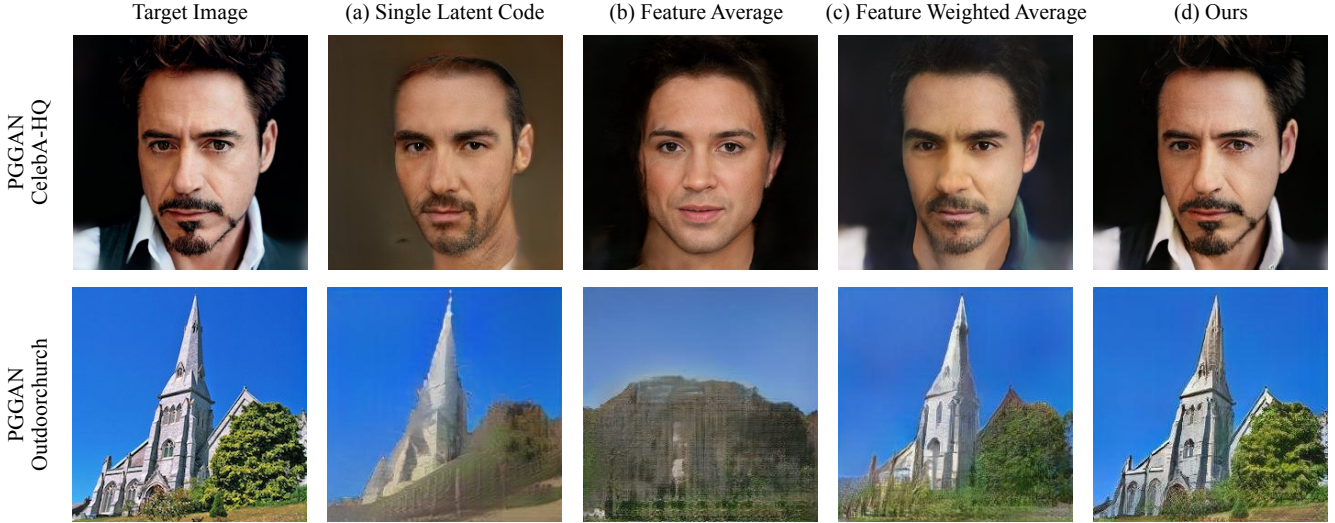


Figure 15: Comparison of different feature composition methods, including (a) directly optimizing a single latent code (no composition), (b) averaging spatial features, (c) weighted averaging spatial features, and (d) our method with adaptive channel importance.

the influence of different layers on the feature composition, we apply our approach on various layers of PGGAN (*i.e.*, from 1st to 8th) to invert 40 images and compare the inversion quality. Fig. 13 shows the comparison results. In general, a higher composition layer could lead to a better inversion effect, as the spatial feature maps contain richer information for reference. However, as revealed in [4],

higher layers contain the information of local pixel patterns such as materials, edges, and colors rather than the high-level semantics. Inverting images into the higher layers is hard to make good use of the learned semantic information of generative networks. It turns out that using 20 latent codes and composing features at the 6th layer is the best option.



### C. More Inversion Results

In this section, we show more inversion results of our method on PGGAN [23] and StyleGAN [24]. Besides inverting PGGAN models trained on various datasets as in Fig.16, our method is also capable of inverting the StyleGAN model which has a style-based generator [24]. In particular, StyleGAN first maps the sampled latent code  $\mathbf{z}$  to a disentangled style code  $\mathbf{w} \in \mathbb{R}^{512}$  before applying it for further generation. This code is then fed into all convolution layers. We can regard these layer-wise style codes as the optimization target and apply our inversion method on these codes to invert StyleGAN. Fig.17 shows that our method helps improve the inversion quality on the StyleGAN model trained for face synthesis.

### D. More Application Results

In this section, we show more results with multi-code GAN prior on various applications. Fig.18 compares our approach to RCAN [48] and ESRGAN [41] on super-resolution task. Fig.19 and Fig.20 shows more colorization and inpainting results respectively. We also apply our method onto real face editing tasks, including semantic manipulation in Fig.21 and style mixing in Fig.22. All these results suggest that we can employ a well-trained GAN model as multi-code prior for a variety of real image processing tasks *without* any retraining.

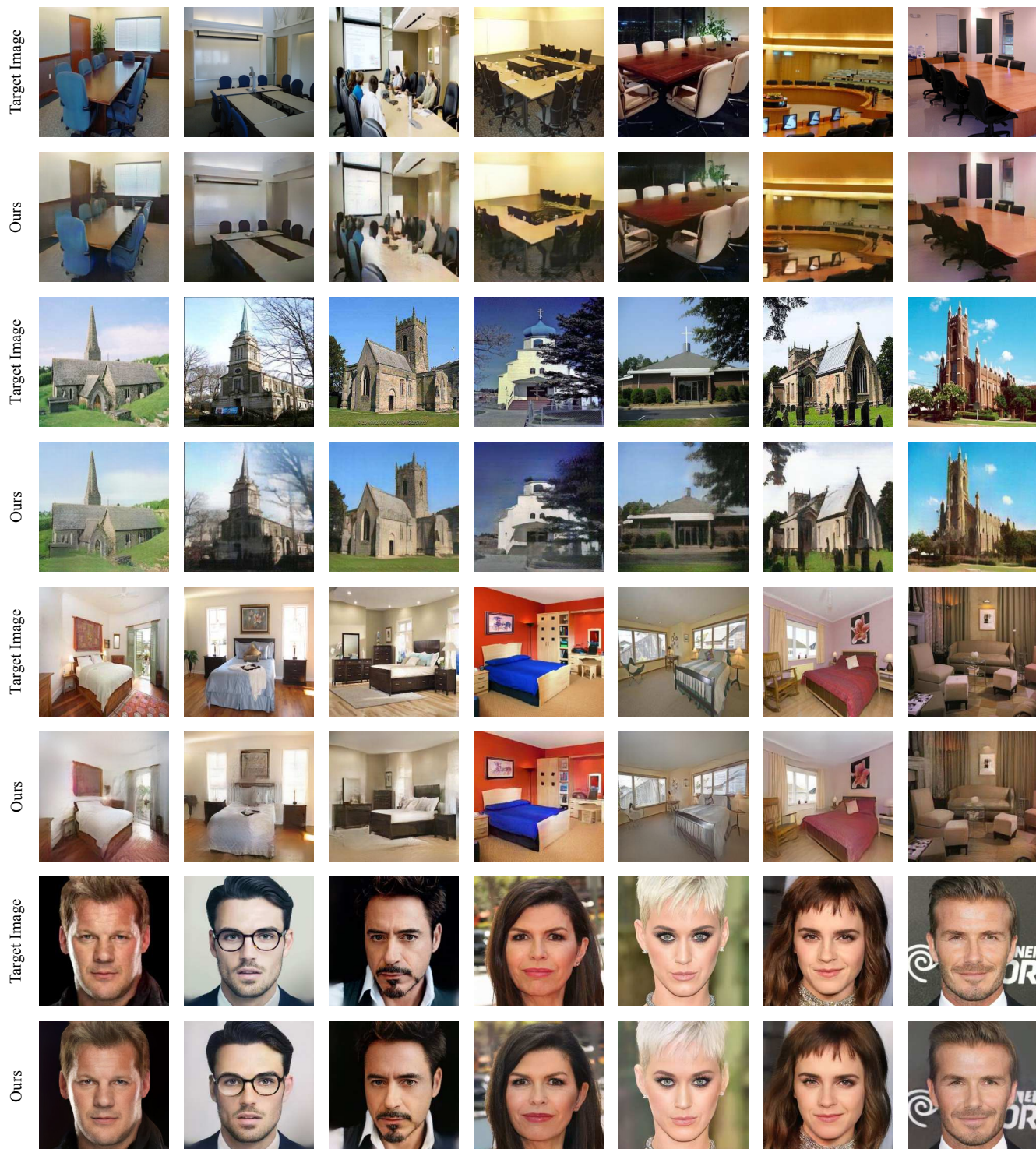


Figure 16: More inversion results with PGGAN [23] models, which are trained to generate images of conference room, outdoor church, bedroom, and human face respectively.



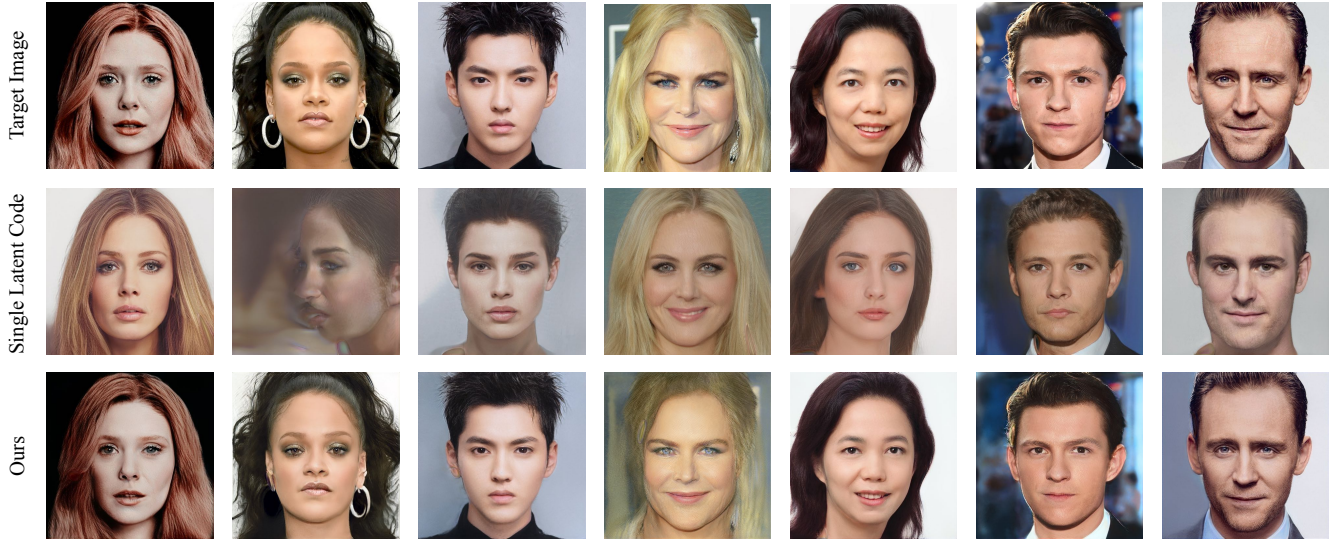


Figure 17: More inversion results on the StyleGAN [24] model trained on FFHQ dataset. From top to bottom: target images, results by optimizing a single latent code, results by our multi-code inversion approach.

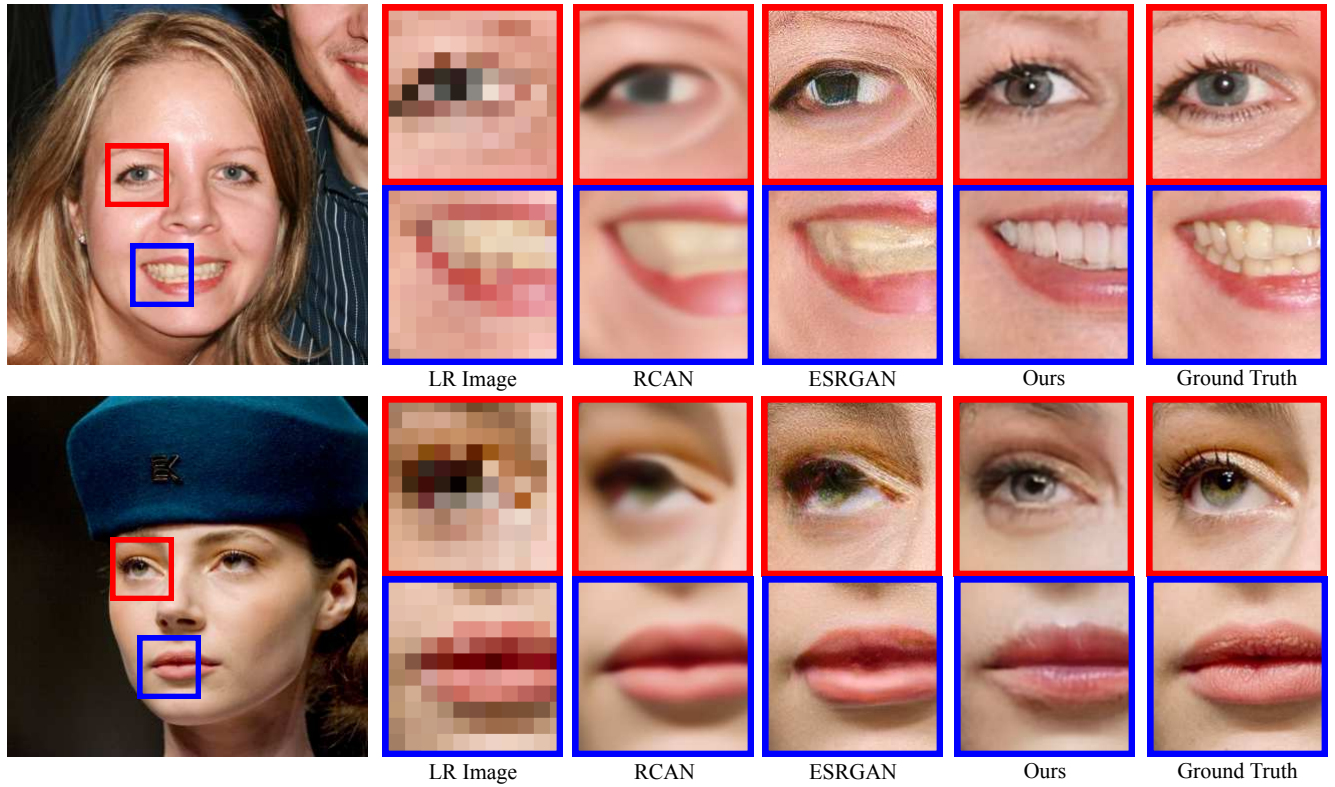


Figure 18: More comparison results between RCAN [48] and ESRGAN [41], and our multi-code GAN prior on super-resolution task with SR factor as 16.



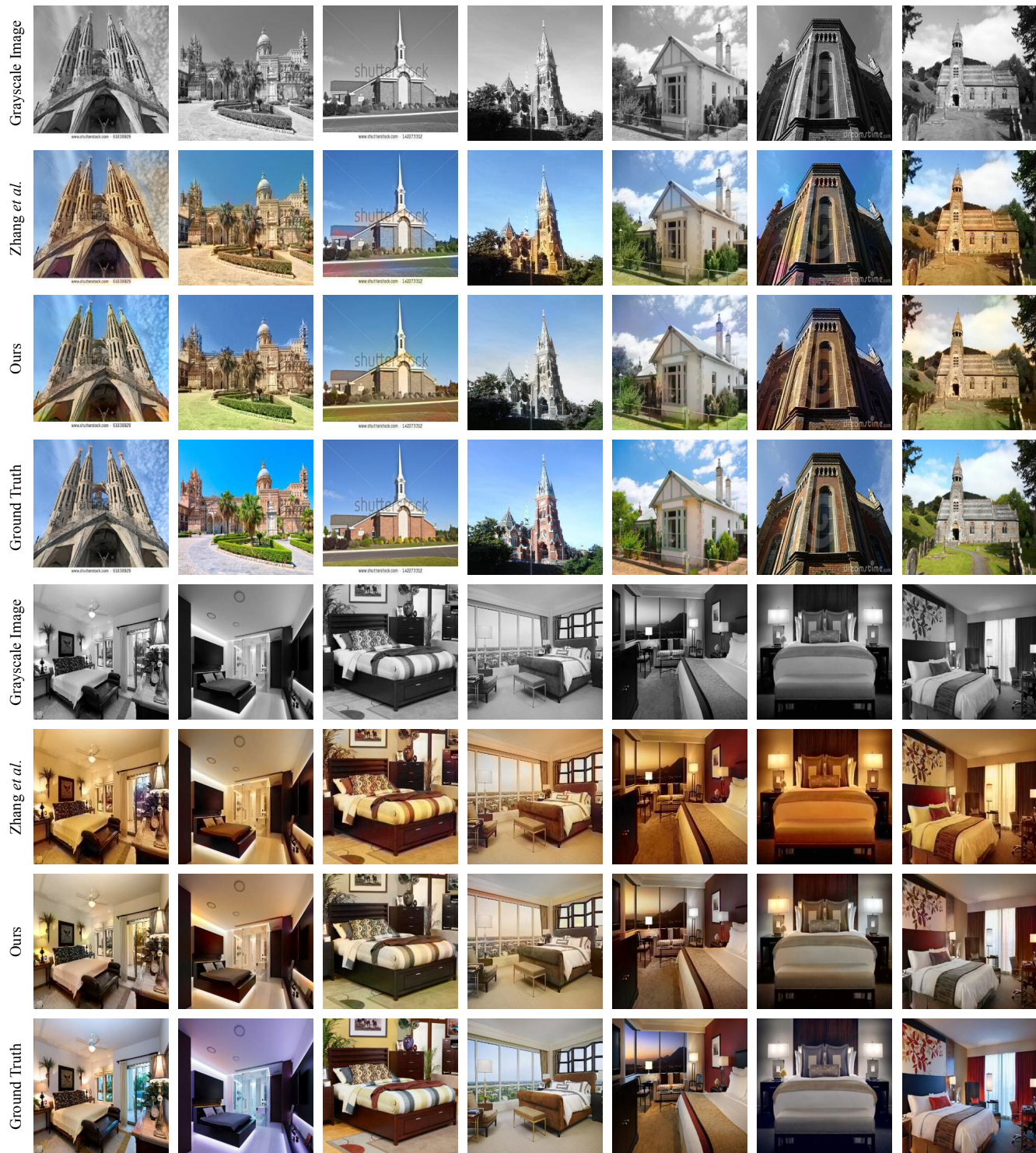


Figure 19: More comparison results between Zhang *et al.* [46] and our multi-code GAN prior on colorization task.





Figure 20: More inpainting results with our method. As can be seen, our method is able to restore the corrupted images by filling in the missing holes with meaningful objects.



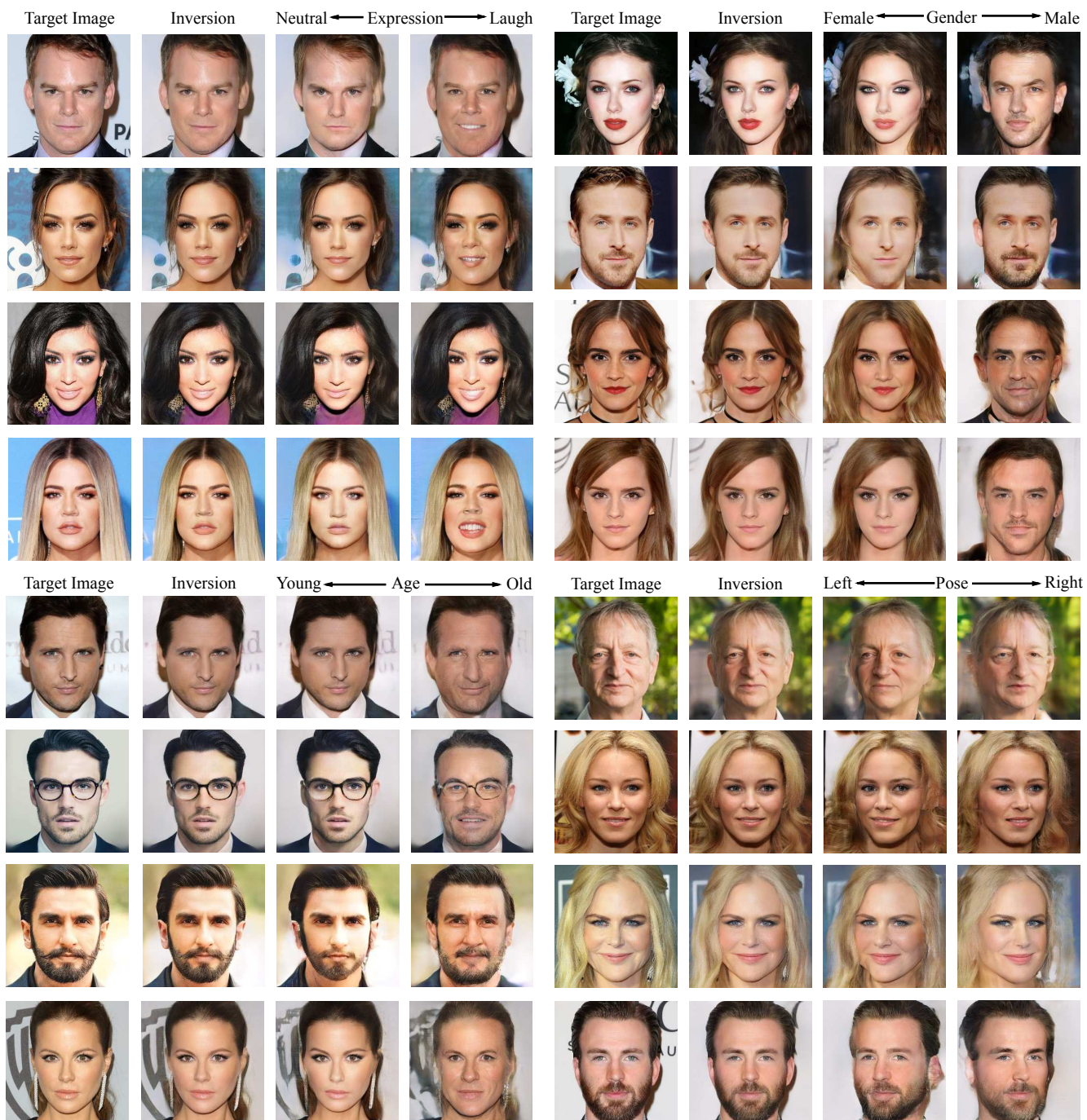


Figure 21: More semantic face manipulation results achieved by multi-code GAN prior. Each image group contains (from left to right) the target real image, the inversion result, and the manipulation results with respect to a particular facial attribute.



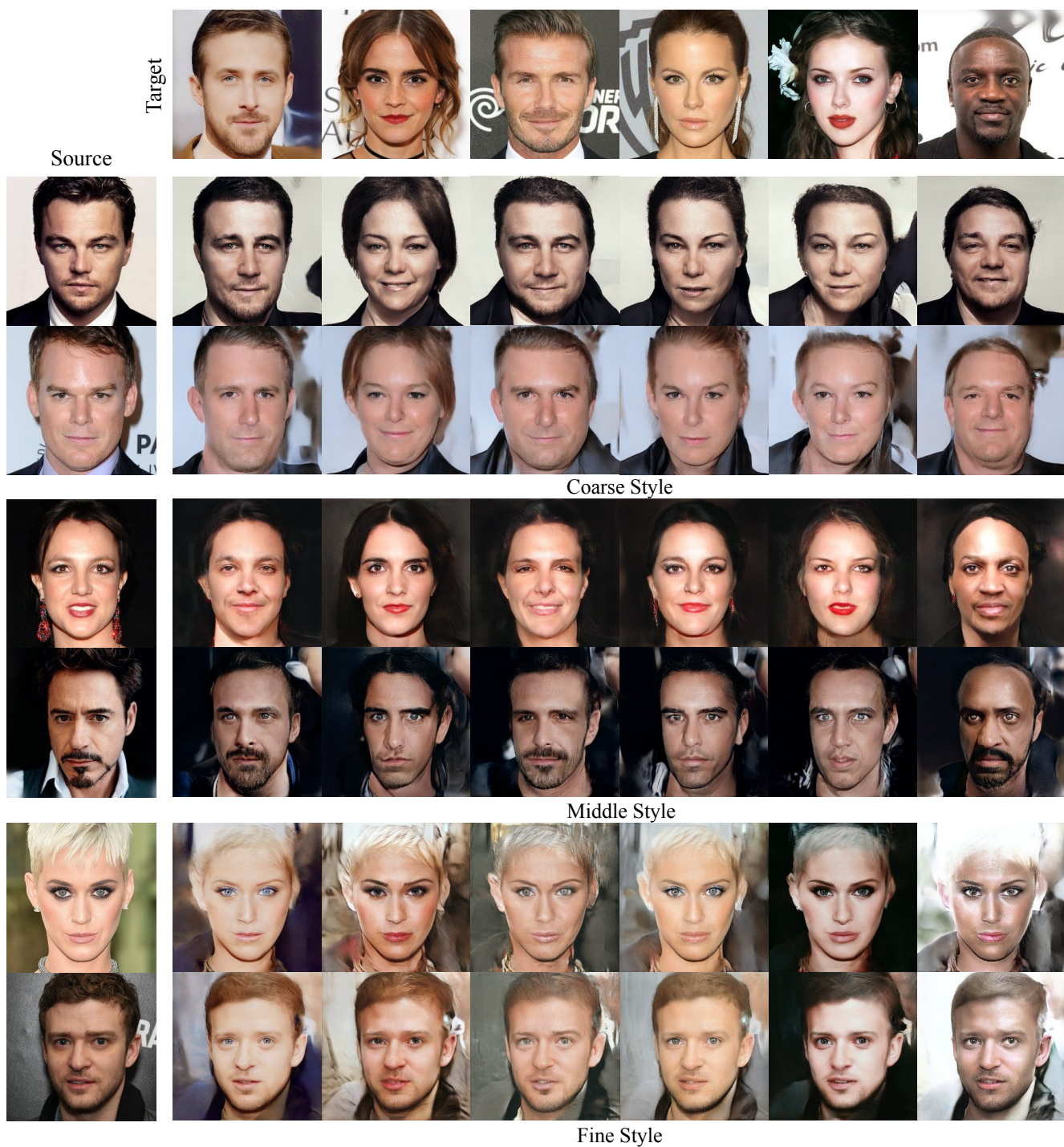


Figure 22: More style mixing results on real faces with StyleGAN [24] model as prior. We copy the inverted style codes from target images to those from source images at different levels, i.e., coarse-level (low-level), middle-level, and fine-level (high-level).